ACS OMEGA

Open Access

http://pubs.acs.org/journal/acsodf

Article

Exploring the Interfacial Formation between Aqueous Slabs and a Hydrophobic Membrane

Orhan Kaya*

Cite This: *ACS Omega* 2025, 10, 18650−18656

Read Online

ACCESS | Metrics & More | Article Recommendations | Supporting Information

ABSTRACT: Molecular dynamics simulations were used to study the interfacial formation between pure and saline aqueous slabs and hydrophobic polytetrafluoroethylene (PTFE) surfaces, both porous and nonporous. The simulations revealed that the formation of transient water vapor bridges between the slabs and the hydrophobic surface facilitated initial contact by lowering the energy barrier, ultimately leading to surface adherence. The presence of saline aqueous slabs slowed the contact process and influenced the dynamics of the vapor-phase bridges. Additionally, porous PTFE surfaces accelerated the initial contact of the aqueous slabs and exhibited distinctive ion concentration gradients, particularly at the pore centers, indicating localized salinity. Structural deformations, such as bending and pore contact angles, were quantified, providing new insights into the nano-structural changes during the interactions between the slabs and PTFE surfaces.

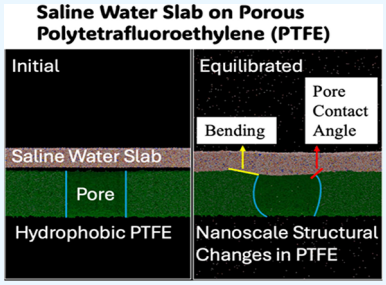

1. INTRODUCTION

The interaction between water and other surfaces, such as quartz and corundum,[1] graphite and silica,[2] alumina,[3] calcite,[4] and graphene,[5] has been studied using MD simulations, revealing that the structuring of interfacial water near these surfaces differs from that in bulk water. The interaction regimes of interfacial water near hydrophilic and hydrophobic surfaces were investigated by Matej Kanduc et al.[6] to explore the potential for designing surface combinations with extremely low or even vanishing contact angles. The relationship between the wetting coefficient, which quantifies a substrate's hydrophobicity, and the density depletion near the solid surface was examined by Jiri Janecek et al.[7] Although these interfaces had been studied in previous work, the effects of porosity on wetting behavior and interfacial formation had not been systematically explored.

In the present study, this gap was addressed by investigating the structural deformations, wetting properties, and ion concentration gradients that arose during water-PTFE interactions to explore an atomistic-level understanding of how aqueous slabs interact with realistically modeled hydrophobic PTFE surfaces—an essential step toward advancing the understanding of fundamental interfacial processes in hydrophobic environments. Insights into the wetting behavior and ion distribution near PTFE surfaces can guide the design of more efficient hydrophobic membranes for applications such as desalination and water purification.[8] Additionally, understanding ion behavior at hydrophobic interfaces can enhance electrochemical systems, including batteries and capacitive deionization technologies.[9]

2. MOLECULAR INTERACTIONS AND SIMULATION CONFIGURATION

MD simulations using LAMMPS[10] were performed to investigate a water slab on a PTFE surface. OVITO[11] and VMD[12] were used for postprocessing. The setup included real units, a full atom style, periodic x and y boundaries, reflective z walls, and a tilted simulation box. Atom interactions were modeled with Lennard-Jones and Coulombic potentials (12 Å cutoff, lj/cut/coul/long pair style), with long-range electrostatics via the PPPM method.[13] Bonded interactions used harmonic (bonds/angles)[14] and OPLS (dihedrals)[15] styles, using the formula

$$u_{ij}(r) = 4\varepsilon_{ij}\left[\left(\frac{\sigma_{ij}}{r}\right)^{12} - \left(\frac{\sigma_{ij}}{r}\right)^{6}\right] + \frac{1}{4\pi\varepsilon_0}\frac{q_i q_j}{r}$$

where r represents the distance between positions i and j, q_i and q_j denote the electric charges at sites i and j, ε_0 is the vacuum permittivity, ε_{ij} is the Lennard-Jones well depth, and σ_{ij} is the characteristic diameter. The mixed pair coefficients between atom types i and j were calculated using the arithmetic mixing rule: $\epsilon_{ij} = \sqrt{\epsilon_i \epsilon_j}$, and $\sigma_{ij} = (\sigma_i + \sigma_j)/2$. The system included F (fluorine) and C (carbon) groups in CF_3 and CF_2 (PTFE), H_2O (water), Na^+ (sodium), and Cl^- (chloride). Bonded, Lennard-Jones, and charge parameters for PTFE were taken from refs 16,

Received: December 31, 2024
Revised: April 19, 2025
Accepted: April 23, 2025
Published: May 2, 2025

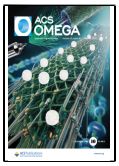

17, with the SPC/E water model[18] used for water. Nonbonded parameters are detailed in Table 1.

Table 1. Lennard−Jones Parameters and Partial Charges for PTFE, Water, and Ions

pair coeffs	σ (nm)	ε (kJ/mol)	q (e)
$F_{(PTFE)}$	2.5378	0.0634	−0.11018
$CF_{3\ (PTFE)}$	2.8062	0.0838	0.33040
$CF_{2\ (PTFE)}$	2.8812	0.0781	0.22050
$O_{(water)}$	3.1655	0.1554	−0.84760
$H_{(water)}$	0.0	0.0	0.42380
$Na^{+}_{(ion)}$	3.3304	0.0027	1
$Cl^{-}_{(ion)}$	4.4172	0.1177	−1

Packmol[19] arranged water and ions with a 2.0 Å spacing, while Na^+ and Cl^- parameters were OPLS-derived[20] from GROMACS.[21] The system was stabilized at 353.15 K using the Nosé−Hoover thermostat,[22] with the velocity-Verlet algorithm (2.0 fs time step) for integration. The concentration of the saline water slab, C_{NaCl}, was calculated from data configurations of water and ion counts from Table 2 using the formula

$$C_{NaCl} = \frac{m_{Na^+} + m_{Cl^-}}{m_{water} + m_{Na^+} + m_{Cl^-}} \times 100\%$$

where m_{Na^+} and m_{Cl^-} are the ion masses, and m_{water} is the water mass.

Table 2. Configurations of Water and Ion Count with C_{NaCl} in Saline and Pure Slabs on Nonporous and Porous PTFE

configurations	N_{water}	N_{Na^+}	N_{Cl^-}	C_{NaCl}
saline slab on nonporous PTFE	1,277,150	36,425	36,425	8.47%
saline slab on porous PTFE	1,277,150	36,425	36,425	8.47%
pure slab on nonporous PTFE	1,350,000	0	0	0%
pure slab on porous PTFE	1,350,000	0	0	0%

The simulation model is depicted in Figure 1. The PTFE chain, structured as CF_3-$(C_2F_4)_n$-CF_3, was based on the force field parameters by Orhan Kaya et al.[16,17] The initial PTFE chain, shown in Figure 1a, includes 50 tetrafluoroethylene (C_2F_4) units capped by CF_3 groups. This polymer chain was constructed using Avogadro[23] and duplicated to form 50 identical chains arranged in a cubic lattice to simulate hydrophobic PTFE. Energy minimization was performed to resolve atomic overlaps, followed by a 5 ns *NPT* MD simulation to compress the structure and achieve the experimental density of 2180 (kg/m^3),[24] as shown in Figure 1b. The PTFE assembly was then extended along the *z*-axis, as shown in Figure 1c and the *x*- and *y*-axes in Figure 1d to enlarge the system. The nonporous enlarged assembly was subjected to a 1 ns *NVT* MD run for equilibration. Surface hydrophobicity was assessed by measuring the contact angles of saline and pure water droplets on the nonporous surface. The contact angle of the pure water droplet (122.86°) closely matched the experimental result reported by Yijie Xiang et al. (122.50°).[25] The contact angle of the saline droplet (130.08°) was recorded; however, no experimental data were available for comparison. The contact angle of the saline droplet (130.08°) was recorded; however, no experimental data were available for comparison.

Detailed results are provided in the Supporting Information section. The methodology for measuring the contact angle was explained by Orhan Kaya.[26] A 24 nm pore was created for porous PTFE. The density at each step from b to f in Figure 1 was analyzed to confirm the presence of only saturated PTFE regions around the pore. Both porous and nonporous PTFE were combined with equilibrated saline and pure water slabs, resulting in four configurations shown in Figure 1e,f. The systems were then run, and the results discussed in the following section.

3. RESULTS AND DISCUSSION

The simulation results were divided into four phases, and the simulations were recorded every 0.25 ns until the final time.

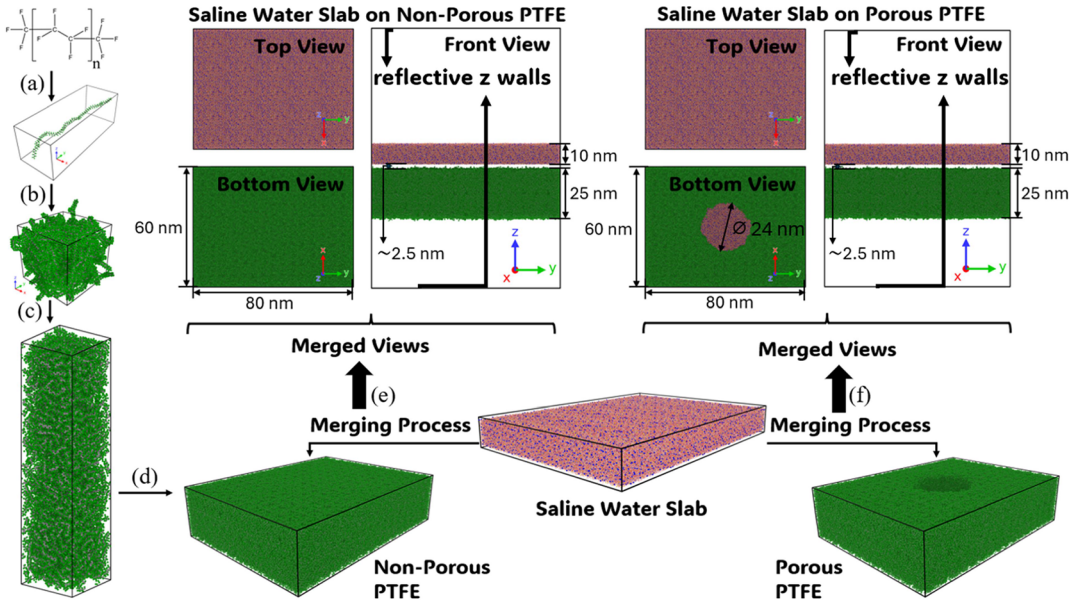

Figure 1. Figure illustrates the PTFE polymer assembly and its merging with saline water slabs. (a) PTFE chain is CF_3-$(C_2F_4)_n$-CF_3 with n = 50. (b) and (c) Chain duplication, minimization, and *z*-axis replication. (d) Fully assembled PTFE along the *x*- and *y*-axes. (e, f) S-water slabs merging with nonporous and porous PTFE, highlighting the 24 nm pore in the porous PTFE.

https://doi.org/10.1021/acsomega.4c11726
ACS Omega 2025, 10, 18650−18656

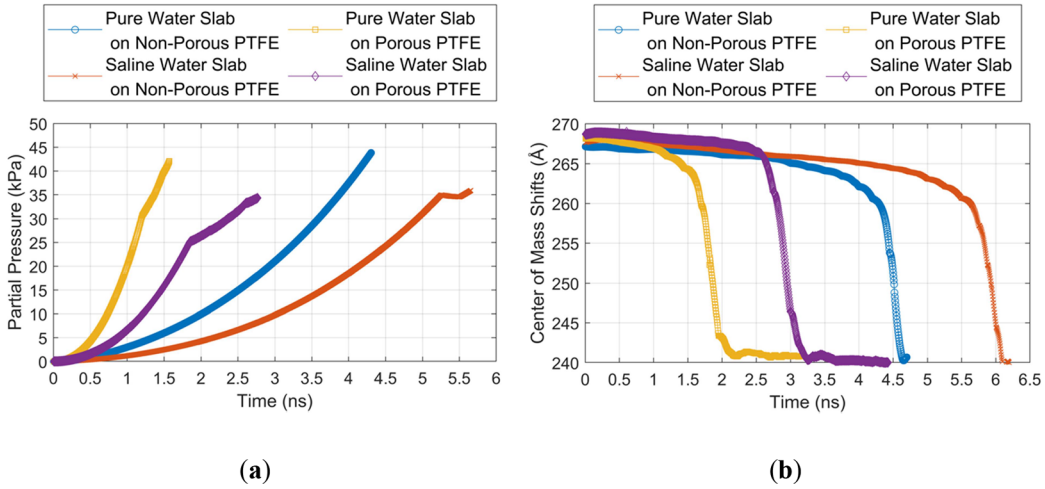

Figure 2. Center of mass shifts (a) and partial pressure variations (b) for pure and saline water slabs on porous and nonporous PTFE surfaces over time.

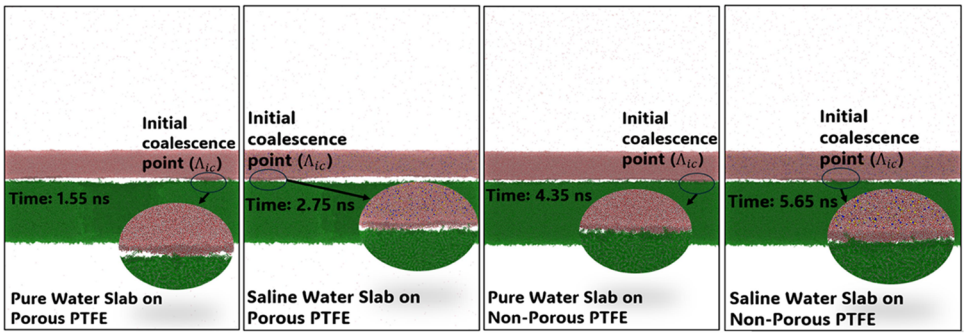

Figure 3. Initial coalescence points and time to contact for pure and saline water slabs on porous and nonporous PTFE surfaces.

Initially, transient vapor bridges formed in the gap enabling contact. The water slab then touched the PTFE surface at the initial coalescence point, where the vapor pressure peaked. Coalescence was observed in the same regions when the simulation was repeated over the coalescence points' time interval. Without a pore, the saline or pure water layer was uniformly displaced downward. Coalescence points formed where vapor-phase bridges created partial pressure peaks. In the porous membrane case, they initially formed an arc at the edges before spreading across the surface. This equilibration process was recorded as a video and can be accessed in the Supporting Information section titled Slabs_on_PTFE.

The analyses were conducted postequilibration, as illustrated by the partial pressure variations calculated using LAMMPS in Figure 2a and the center of mass shifts calculated using OVITO in Figure 2b. The simulations were recorded at 0.25 ns intervals until the final time is shown in Figure 2a. Density analysis of the interfacial gap was performed at these intervals to identify regions where the density had fallen below 0.5 (g/cm^3).[27] The interfacial gap was then defined as a rectangular region in LAMMPS, and the partial pressure within this region was calculated by using the ideal gas law. The number of gas molecules in the interfacial gap was determined from the molecular distribution in the simulation data. By applying this methodology at each recorded time step, a time-resolved analysis of the partial pressure evolution in the interfacial gap was obtained. The partial pressure increased steadily as more bridges formed, while the slabs moved closer to the PTFE surface. The moments when pressure peaked corresponded to the initial coalescence, indicating the collapse of the vapor bridges, shown as a sharp decline in Figure 2b, and the beginning of contact nucleation depicted in Figure 3. Following this, the contact nucleation points spread across the surface, rapidly drawing the water slab closer to the PTFE surface.

As shown in Figure 2b, the center of mass shifts show that contact nucleation occurred faster on porous PTFE than on nonporous surfaces. The comparison also revealed that salinity slowed the contact process by altering vapor-phase bridge dynamics and prolonging their persistence, complicating the interaction with hydrophobic surfaces. Density profiles and wetting interfaces for pure water slabs on nonporous and porous PTFE surfaces were analyzed after equilibration, as shown in Figure 4. The initial wetting interface marked the first wetting point, while the solid−liquid dividing interface indicated where PTFE roughness ended and full wetting began. On porous PTFE, initial wetting occurred earlier due to water bending around the pores, as seen in Figure 4a,b. Thus, wetting was uniform on nonporous PTFE but gradually spread around the pores on the porous surface, resulting in broader wetting. This behavior is reflected in the different wetting ranges, with 16.5 Å for the nonporous case and 20.75 Å for the porous case in Figure 4.

The resulting changes in PTFE's morphological structure are shown schematically in Figure 5a, with the initial and final deformations of the PTFE surface affected by the pure slab in Figure 5b and the saline slab in Figure 5c. OVITO's surface detection algorithm, which uses the alpha shape method—a generalized version of the convex hull—was applied to construct

https://doi.org/10.1021/acsomega.4c11726
ACS Omega 2025, 10, 18650−18656

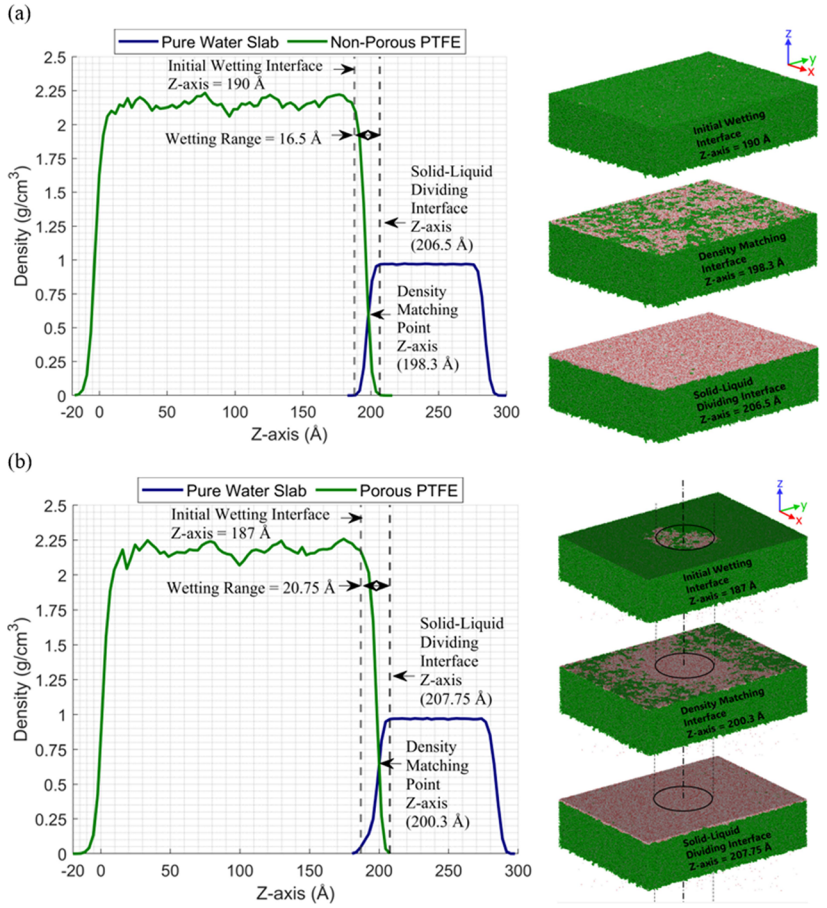

Figure 4. Comparison of density profiles and wetting interfaces between (a) pure water slab on nonporous and (b) porous PTFE surfaces.

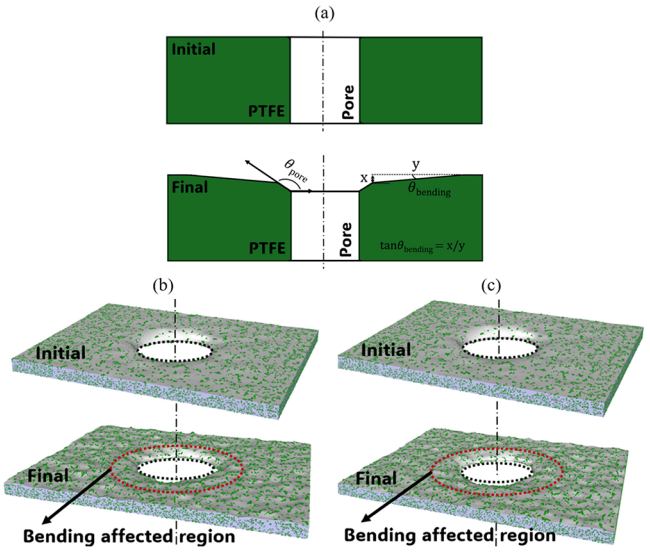

Figure 5. (a) Illustration of slab-induced bending and pore contact angles in PTFE before and after deformation. (b) PTFE surface deformation before and after contact with the pure slab. (c) PTFE surface deformation before and after contact with the saline slab.

a surface mesh for visualizing surface deformation. Analysis of the initial and final deformations revealed the pore contact and bending angles as two key structural changes in the PTFE surface.

The bending angle ($\theta_{bending}$) represents the overall bending or warping of the PTFE surface around the pore due to the forces exerted by the slab. The bending angle was formed due to the curvature of the PTFE surface in the pore region. This curvature resulted from the applied force of the slabs and was expressed as the slope of the PTFE surface. In Figure 5a, $\theta_{bending}$ is depicted between the horizontal plane (x-axis) and the sloped PTFE surface after deformation. The equation ($\tan(\theta_{bending}) = x/y$) describes the relationship between the horizontal distance (x) over which the surface deformed and the vertical distance (y) of the bending. This equation enables the calculation of the bending angle from the trajectory file. For the PTFE surface affected by the pure slab, $\theta_{bending}$ was approximately 8°. For the surface influenced by the saline slab, the $\theta_{bending}$ was approximately 11°.

Pore contact angles θ_{pore}, shown in Figures 5a and 6c, reflected the deformation of the pore's sidewalls. This angle, formed between the vertical axis of the pore and its sloping sidewalls after deformation, indicated the change in sidewall orientation due to the slab's influence on the PTFE structure.

Initially, the pore walls were nearly vertical. After deformation, they tilted inward or outward, altering this angle. The angle was calculated by using a cylindrical coordinate system centered on the pore, Figure 6a, with the final point of the water/vapor interface curve defining the water slab edge. The angle was measured by fitting a curve to the interface and finding the tangent at the pore edge, Figure 6b. Four different contact angles were measured in Table 3 for each slab at distinct points illustrated in Figure 6a around the pore, labeled $\theta_{I°}$, $\theta_{II°}$, $\theta_{III°}$, and

https://doi.org/10.1021/acsomega.4c11726
ACS Omega 2025, 10, 18650−18656

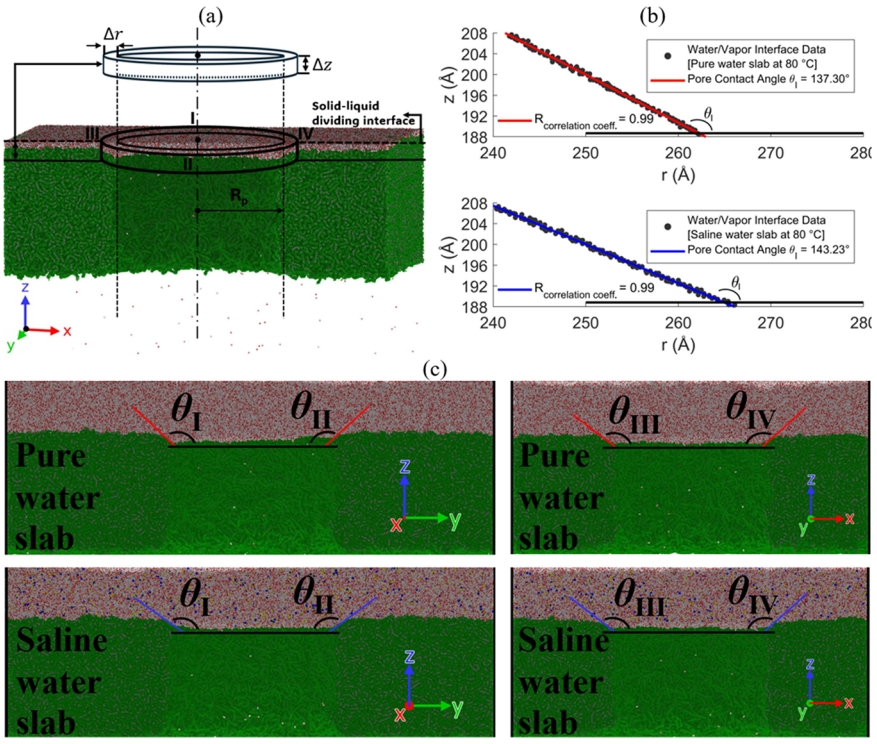

Figure 6. Calculation method for pore contact angles: (a) Establishment of the cylindrical coordinate system. (b) Water/vapor interface data and pore contact angle determination for pure and saline water slabs. (c) Comparison of contact angles (θ) at different pore regions for pure and saline water slabs.

Table 3. Averaged Pore Contact Angle Measurements for Pure and Saline Water Slabs

configurations	T (°C)	$\theta_{I°}$	$\theta_{II°}$	$\theta_{III°}$	$\theta_{IV°}$	angle°
saline slab on porous PTFE	80	137.30	139.08	144.58	138.79	139.94
pure slab on porous PTFE	80	143.23	144.78	142.76	140.65	142.86

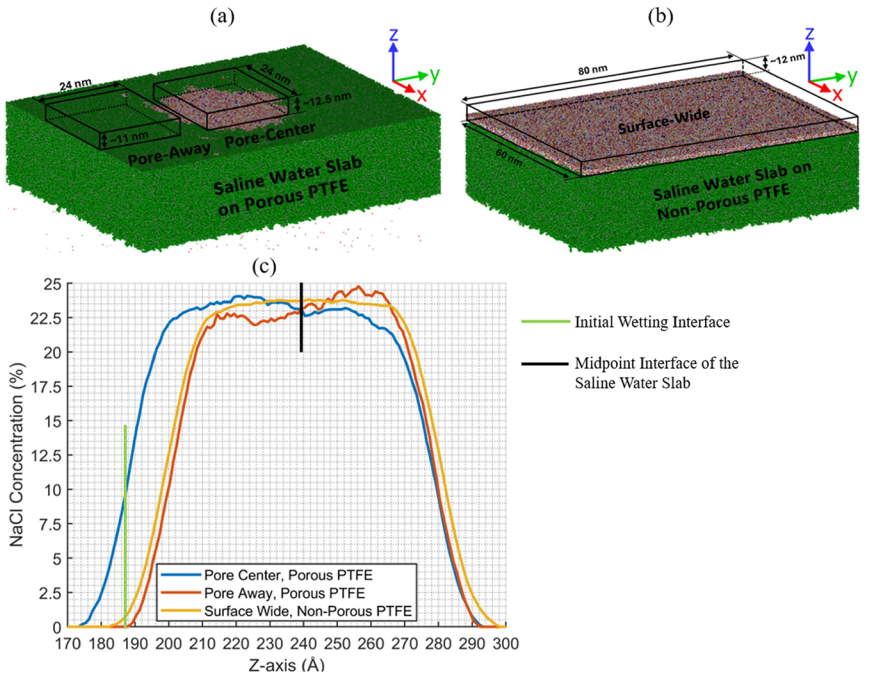

Figure 7. NaCl concentration in saline water slabs on porous and nonporous PTFE: (a) Pore-center and pore-away regions on porous PTFE. (b) Surface-wide sampling on nonporous PTFE. (c) NaCl concentration profiles along the Z-axis.

https://doi.org/10.1021/acsomega.4c11726
ACS Omega 2025, 10, 18650−18656

θ_{IV° in Figure 6c. By averaging these angles, the contact angle for the pure water slab was calculated as θ_{pure} = 139.94 and for the saline water slab as θ_{saline} = 142.86.

The ion concentration profiles of NaCl in saline water slabs on porous and nonporous PTFE surfaces were analyzed. Figure 7a,b highlights distinct regions: Pore-Center and Pore-Away zones on porous PTFE, and Surface-Wide distribution on nonporous PTFE. Figure 7c shows that, on nonporous PTFE, ion distribution was homogeneous with a smooth increase near the surface. In contrast, porous PTFE showed ion accumulation at the Pore-Center was higher than the Pore-Away region, indicating localized salinity due to the pore's influence. Starting from the Initial Wetting Interface to the Midpoint Interface of the Saline Water Slab, less accumulation of NaCl was observed in the Pore-Away region compared to the Surface-Wide region for every *Z*-axis value, suggesting that pore effects extend beyond direct contact areas.

These findings suggest that surface porosity significantly impacts the ion behavior, extending its influence beyond the immediate vicinity of the pores. The simulation results demonstrated localized salinity, particularly at the Pore-Center of the Porous PTFE surface. In contrast, the nonporous PTFE surface exhibited a more uniform ion distribution with less pronounced localization. The presence of pores enhanced ion accumulation near the surface, consistent with ion localization resulting from restricted diffusion of ions from the interfacial region.

4. CONCLUSIONS

This study provided new insights into the interfacial formation of water on hydrophobic PTFE surfaces. The identification of transient water vapor bridges as intermediate structures demonstrated their role in lowering the energy barrier for contact and stabilizing the system during equilibration, marked by center of mass shifts. This newly observed mechanism introduces a unique stabilizing element not previously reported in MD simulations. Additionally, tracking partial pressure within the interfacial gap revealed peaks that signaled coalescence timing, opening new avenues for investigating the thermodynamics of nucleation at hydrophobic interfaces. The analysis also underscored the influence of the surface morphology on wetting behavior. Porous and nonporous PTFE surfaces showed differing effects on interfacial water density and wetting distributions, leading to structural deformations such as bending and pore-specific contact angles. Finally, a novel perspective on localized salinity was presented through the spatial analysis of NaCl distribution in porous PTFE. The significant ion accumulation in the Pore-Center region and resulting sharp gradients revealed the impact of porosity on ion distribution, enhancing the understanding of interfacial behaviors and contributing valuable insights into wettability and ion segregation near hydrophobic interfaces.

■ ASSOCIATED CONTENT

Supporting Information

The Supporting Information is available free of charge at https://pubs.acs.org/doi/10.1021/acsomega.4c11726.

Slabs_on_PTFE (MP4)

Degree of surface hydrophobicity of droplets on a nonporous PTFE surface at 80 °C under both pure and saline conditions (PDF)

■ AUTHOR INFORMATION

Corresponding Author

Orhan Kaya − *Department of Mechanical Engineering and Mechanics, Lehigh University, Bethlehem, Pennsylvania 18015, United States;* orcid.org/0000-0002-5994-3500; Email: ork216@lehigh.edu

Complete contact information is available at: https://pubs.acs.org/10.1021/acsomega.4c11726

Funding

This research received no external funding.

Notes

The author declares no competing financial interest.

■ ACKNOWLEDGMENTS

The results were obtained using Texas A&M's FASTER, under ACCESS MCH220041 support.

■ REFERENCES

(1) Quezada, G. R.; Rozas, R. E.; Toledo, P. G. Molecular Dynamics Simulations of Quartz (101)−Water and Corundum (001)−Water Interfaces: Effect of Surface Charge and Ions on Cation Adsorption, Water Orientation, and Surface Charge Reversal. *J. Phys. Chem. C* **2017**, *121* (45), 25271−25282.

(2) Argyris, D.; Tummala, N. R.; Striolo, A.; Cole, D. R. Molecular Structure and Dynamics in Thin Water Films at the Silica and Graphite Surfaces. *J. Phys. Chem. C* **2008**, *112* (35), 13587−13599.

(3) Argyris, D.; Ho, T.; Cole, D. R.; Striolo, A. Molecular Dynamics Studies of Interfacial Water at the Alumina Surface. *J. Phys. Chem. C* **2011**, *115* (5), 2038−2046.

(4) Ali, A.; Le, T. T. B.; Striolo, A.; Cole, D. R. Salt Effects on the Structure and Dynamics of Interfacial Water on Calcite Probed by Equilibrium Molecular Dynamics Simulations. *J. Phys. Chem. C* **2020**, *124* (45), 24822−24836.

(5) Garcia, R. Interfacial Liquid Water on Graphite, Graphene, and 2D Materials. *ACS Nano* **2023**, *17* (1), 51−69.

(6) Kanduč, M.; Schlaich, A.; Schneck, E.; Netz, R. R. Water-Mediated Interactions between Hydrophilic and Hydrophobic Surfaces. *Langmuir* **2016**, *32* (35), 8767−8782.

(7) Janeček, J.; Netz, R. R. Interfacial Water at Hydrophobic and Hydrophilic Surfaces: Depletion versus Adsorption. *Langmuir* **2007**, *23* (16), 8417−8429.

(8) Turk, O. K.; Zoungrana, A.; Cakmakci, M. Performances of PTFE and PVDF Membranes in Achieving the Discharge Limit of Mixed Anodic Oxidation Coating Wastewaters Treated by Membrane Distillation. *Environ. Sci. Pollut. Res.* **2024**, *31* (27), 39663−39677.

(9) Devlin, S. W.; Benjamin, I.; Saykally, R. J. On the Mechanisms of Ion Adsorption to Aqueous Interfaces: Air-Water vs. *Oil-Water. Proc. Natl. Acad. Sci.* **2022**, *119* (42), No. e2210857119.

(10) Thompson, A. P.; Aktulga, H. M.; Berger, R.; Bolintineanu, D. S.; Brown, W. M.; Crozier, P. S.; In'T Veld, P. J.; Kohlmeyer, A.; Moore, S. G.; Nguyen, T. D.; Shan, R.; Stevens, M. J.; Tranchida, J.; Trott, C.; Plimpton, S. J. LAMMPS - a Flexible Simulation Tool for Particle-Based Materials Modeling at the Atomic, Meso, and Continuum Scales. *Comput. Phys. Commun.* **2022**, *271*, No. 108171.

(11) Stukowski, A. Visualization and Analysis of Atomistic Simulation Data with OVITO−the Open Visualization Tool. *Model. Simul. Mater. Sci. Eng.* **2010**, *18* (1), No. 015012.

(12) Humphrey, W.; Dalke, A.; Schulten, K. VMD: Visual Molecular Dynamics. *J. Mol. Graph.* **1996**, *14* (1), 33−38.

(13) Darden, T.; York, D.; Pedersen, L. Particle Mesh Ewald: An N · log(N) Method for Ewald Sums in Large Systems. *J. Chem. Phys.* **1993**, *98* (12), 10089−10092.

(14) Andersen, H. C. Rattle: A "Velocity" Version of the Shake Algorithm for Molecular Dynamics Calculations. *J. Comput. Phys.* **1983**, *52* (1), 24−34.

(15) Watkins, E. K.; Jorgensen, W. L. Perfluoroalkanes: Conformational Analysis and Liquid-State Properties from Ab Initio and Monte Carlo Calculations. *J. Phys. Chem. A* **2001**, *105* (16), 4118−4125.
(16) Kaya, O.; Oztekin, A.; Webb, E. B. Development of AMBER-Compliant Transferable Force Field Parameters for Polytetrafluoroethylene. *Open Chem.* **2024**, *22* (1), 20240072.
(17) Kaya, O. Data from "Development of an AMBER-Compliant Transferable Force Field Parameters for Polytetrafluoroethylene," 2024, 322406 Bytes. .
(18) Berendsen, H. J. C.; Grigera, J. R.; Straatsma, T. P. The Missing Term in Effective Pair Potentials. *J. Phys. Chem.* **1987**, *91* (24), 6269−6271.
(19) Martínez, L.; Andrade, R.; Birgin, E. G.; Martínez, J. M. P ACKMOL: A Package for Building Initial Configurations for Molecular Dynamics Simulations. *J. Comput. Chem.* **2009**, *30* (13), 2157−2164.
(20) Jorgensen, W. L.; Maxwell, D. S.; Tirado-Rives, J. Development and Testing of the OPLS All-Atom Force Field on Conformational Energetics and Properties of Organic Liquids. *J. Am. Chem. Soc.* **1996**, *118* (45), 11225−11236.
(21) Abraham, M. J.; Murtola, T.; Schulz, R.; Páll, S.; Smith, J. C.; Hess, B.; Lindahl, E. GROMACS: High Performance Molecular Simulations through Multi-Level Parallelism from Laptops to Supercomputers. *SoftwareX* **2015**, *1−2*, 19−25.
(22) Nosé, S. A Molecular Dynamics Method for Simulations in the Canonical Ensemble. *Mol. Phys.* **1984**, *52* (2), 255−268.
(23) Hanwell, M. D.; Curtis, D. E.; Lonie, D. C.; Vandermeersch, T.; Zurek, E.; Hutchison, G. R. Avogadro: An Advanced Semantic Chemical Editor, Visualization, and Analysis Platform. *J. Cheminformatics* **2012**, *4* (1), 17.
(24) Nunes, L. C. S.; Dias, F. W. R.; Da Costa Mattos, H. S. Mechanical Behavior of Polytetrafluoroethylene in Tensile Loading under Different Strain Rates. *Polym. Test.* **2011**, *30* (7), 791−796.
(25) Xiang, Y.; Fulmek, P.; Platz, D.; Schmid, U. Temperature Dependence of Water Contact Angle on Teflon AF1600. *Langmuir* **2022**, *38* (4), 1631−1637.
(26) Kaya, O. Hydrophobic Membrane Wettability: Effects of Salinity and Temperature. *Membranes* **2025**, *15* (2), 58.
(27) Park, J. H.; Aluru, N. R. Temperature-Dependent Wettability on a Titanium Dioxide Surface. *Mol. Simul.* **2009**, *35* (1−2), 31−37.

https://doi.org/10.1021/acsomega.4c11726
ACS Omega 2025, 10, 18650−18656